Bispectral Analysis of Overnight Airflow to Improve the Pediatric Sleep Apnea Diagnosis

Verónica Barroso-García[a,b]*, Gonzalo C. Gutiérrez-Tobal[a,b], Leila Kheirandish-Gozal[c], Fernando Vaquerizo-Villar[a,b], Daniel Álvarez[a,b,d], Félix del Campo[a,b,d], David Gozal[c], and Roberto Hornero[a,b]

[a] Biomedical Engineering Group, University of Valladolid, Valladolid, Spain.

[b] CIBER-BBN, Centro de Investigación Biomédica en Red en Bioingeniería, Biomateriales y Nanomedicina, Valladolid, Spain.

[c] Department of Child Health, The University of Missouri School of Medicine, Columbia, Missouri, USA.

[d] Sleep-Ventilation Unit, Pneumology Department, Río Hortega University Hospital, Valladolid, Spain.

* Corresponding author: **Verónica Barroso-García**

Biomedical Engineering Group, E.T.S. Ingenieros de Telecomunicación, Universidad de Valladolid, Campus Miguel Delibes, Paseo Belén 15, 47011 – Valladolid, Spain.

Tel. +34 983 423000 ext. 4713

E-mail address: veronica.barroso@gib.tel.uva.es

URL: www.gib.tel.uva.es

Abstract- Pediatric Obstructive Sleep Apnea (OSA) is a respiratory disease whose diagnosis is performed through overnight polysomnography (PSG). Since it is a complex, time-consuming, expensive, and labor-intensive test, simpler alternatives are being intensively sought. In this study, bispectral analysis of overnight airflow (AF) signal is proposed as a potential approach to replace PSG when indicated. Thus, our objective was to characterize AF through bispectrum, and assess its performance to diagnose pediatric OSA. This characterization was conducted using 13 bispectral features from 946 AF signals. The oxygen desaturation index ≥3% (*ODI*3), a common clinical measure of OSA severity, was also obtained to evaluate its complementarity to the AF bispectral analysis. The fast correlation-based filter (FCBF) and a multi-layer perceptron (MLP) were used for subsequent automatic feature selection and pattern recognition stages. FCBF selected 3 bispectral features and *ODI*3, which were used to train an MLP model with ability to estimate apnea-hypopnea index (AHI). The model reached 82.16%, 82.49%, and 90.15% accuracies for the common AHI cut-offs 1, 5, and 10 events/h, respectively. The different bispectral approaches used to characterize AF in children provided complementary information. Accordingly, bispectral analysis showed that the occurrence of apneic events decreases the non-gaussianity and non-linear interaction of the AF harmonic components, as well as the regularity of the respiratory patterns. Moreover, the bispectral information from AF also showed complementarity with *ODI*3. Our findings suggest that AF bispectral analysis may serve as a useful tool to simplify the diagnosis of pediatric OSA, particularly for children with moderate-to-severe OSA.

Keywords- Adaptive band, Airflow, Bispectrum, Children, Obstructive Sleep Apnea.

1. INTRODUCTION

Obstructive Sleep Apnea (OSA) is a frequent respiratory condition that is present in 5% of children aged 2-18 [1]. Affected children manifest recurrent apnea and/or hypopnea episodes during sleep [2,3]. In children, an apnea reflects complete cessation of airflow during at least 2 respiratory cycles, while a hypopnea is a significant reduction of airflow for two or more breaths and accompanied by a blood oxygen hemoglobin desaturation $\geq$ 3% or an electroencephalographic arousal [3]. Due to the serious consequences that OSA may cause in pediatric subjects, such as cognitive and behavioral deficits and cardiovascular alterations [1], it is of paramount importance to reach an early diagnosis and enable access to treatment.

Overnight polysomnography (PSG) is the standard method used by physicians to diagnose pediatric OSA [4]. This test consists in monitoring the child during sleep using various body sensors to record multiple physiological signals, such as photoplethysmography (PPG), electrocardiogram (ECG), electroencephalography (EEG), oximetry (SpO_2), or airflow (AF), among others [4]. These signals are qualitatively assessed by physicians to obtain the apnea-hypopnea index (AHI: number of apneic and hypopneic events per hour of sleep) and determine OSA severity [2,5]. Nonetheless, PSG is a very complex and time-consuming test, as it requires spending the night in a sleep laboratory and subsequent evaluation of all the physiological data acquired [6]. Moreover, the required facilities to perform complete PSG are not always available, thereby leading to long waiting lists [6]. In order to overcome these drawbacks, possible alternatives to PSG have been evaluated. In this regard, it has been found that home respiratory polygraphy (HRP) could be useful to diagnose pediatric OSA when PSG is not available [7]. In addition, other simpler approaches that involve fewer channels than PSG and HRP have also been assessed. These approaches, based on the

analysis of a reduced set of physiological signals, could help to diagnose the disease and reduce the complexity and intrusion of the diagnostic test. Thus, those signals involved in the PSG, such as ECG, PPG, SpO_2 or AF, are commonly used to this purpose [8–15].

In this study, we planned the automated analysis of the single-channel AF signal to aid in pediatric OSA diagnosis. The AF signal can be obtained using a type IV portable device that incorporates thermistor [16,17]. These devices just use one or two sensors to record one or two physiological parameters, so in addition to simplifying the diagnostic test it would be less uncomfortable for children. Moreover, type IV devices can be used at patient's home, which would streamline diagnosis and reduce waiting lists. According to the definition of OSA, AF shows respiratory alterations due to apneic and hypopneic events [3], leading to changes that can be measured in time- (amplitude-reduction) and frequency- (spectrum-modification) domains, as well as in its phase [3,13–15,18]. This makes AF analysis a promising approach to simplify the diagnosis and potentially obviate the need for PSG. In addition, 3% oxygen desaturation index (*ODI*3) has been computed in our study. This index is directly obtained from the SpO_2 signal [19], and is clinically used to diagnose OSA when PSG availability is limited [20]. However, it is well-known that this index underestimates the severity of OSA [21,22]. In this regard, we also propose to evaluate the complementarity of the *ODI*3 with the AF information.

The recurrent presence of respiratory events during sleep leads to modifications in AF spectrum [18]. Consequently, AF spectral analysis has been widely used in the diagnosis of OSA [14,15,18,23]. This analysis is usually carried out by means of power spectral density (PSD). However, conventional methods of PSD estimation have several limitations, such as the assumption of stationarity and linearity [24,25]. AF is a dynamic, non-linear and non-stationary signal [13]. Consequently, a regular spectral analysis may not provide sufficient information in the pediatric OSA context. In contrast, bispectrum

analysis can reveal changes of linearity and stationarity [26]. Moreover, this method preserves both the amplitude and phase information of the signal [12,26,27]. This property may allow for detection of dependency relationships between different frequencies that are generated by the occurrence of respiratory events, which would not be possible with a conventional spectral analysis [12]. Bispectrum has shown its usefulness to characterize other OSA-related biomedical signals, such as SpO_2 [12], EEG [28], and ECG [29]. However, this is the first time that bispectrum is used to characterize AF in children and estimate their AHI. Based on the aforementioned considerations, our starting hypothesis is that the bispectrum of AF contains OSA-related information. Thus, our main objective is to characterize AF by means of bispectrum, as well as to assess its potential usefulness to determine the presence and severity of OSA in children. In addition, we evaluate the complementarity between AF and the *ODI*3 as a secondary objective. In order to reach these goals, we firstly extracted bispectral features from AF, as well as *ODI*3 from oximetry. Then, the fast correlation-based filter (FCBF) algorithm was applied to select a subset of relevant and non-redundant features. Finally, a multi-layer perceptron (MLP) neural network was trained using this optimum feature subset in order to estimate the AHI.

2. SUBJECTS AND SIGNALS

This study involves 946 subjects aged 0 to 13 years old. All of them were referred to the Paediatric Sleep Unit at the Comer Children's Hospital of the University of Chicago (Chicago, IL, USA) due to clinical OSA suspicion. The informed consents of all children caretakers were obtained, and the Ethics Committee of the Comer Children's Hospital approved the protocol (#11-0268-AM017, #09-115-B-AM031, and #IRB14-1241).

All subjects underwent PSG using a digital polysomnographic system (Polysmith, Nihon Kohden America Inc., Irvine, CA, USA). They were diagnosed by medical specialists following the American Academy of Sleep Medicine (AASM) rules to score apnea and hypopnea events [3]. Thus, based on the analysis of the PSG signals, AHI was obtained to determine the severity of the disease according to the cut-offs commonly used in children: 1, 5, and 10 events/h [2,13,30,31]. Accordingly, the range of AHI < 1 event/h was considered no-OSA, while the ranges 1 event/h ≤ AHI < 5 events/h, 5 events/h ≤ AHI < 10 events/h, and AHI ≥ 10 events/h, were designated as mild, moderate, and severe OSA, respectively.

Children were randomly allocated into two groups: training and test sets. Table 1 displays the clinical and demographic data of the children involved in our study. The continuous variables (age, body mass index, and AHI) did not pass the Lilliefors normality test. Thus, the non-parametric Mann-Whitney *U* test for continuous variables (age, body mass index, and AHI) and the Fisher's exact test for categorical variables (gender and severity groups) were applied, showing no statistically significant differences (*p*-value > 0.01) in any of these parameters between the training and test sets.

PLEASE, DISPLAY TABLE 1 AROUND HERE

AF recordings were acquired by means of a thermistor during PSG. Those recordings lasting less than 3 hours were excluded from the study [13,32]. 946 signals of AF were preprocessed for resampling (100 Hz), removing artifacts, and standardization [13,14]. The *ODI*3 was obtained from the corresponding 946 SpO_2 signals. These signals were also preprocessed for resampling (25 Hz) and artifact removal [12,31]. Figure 1(a) and 1(b) show an example of AF signal before and after the preprocessing stage, respectively. As can be seen, the artifacts (signal loss: 0 to 1.2 minute; noise: 4.3 to 4.7 minute) are removed after AF preprocessing. The raw and preprocessed SpO_2 signals are

also shown in Figure 1(c) and 1(d), respectively. It can be observed that its artifacts (0 to 0.6 hour and around 2.6, 3.6, 4.5, and 7.8 hour) are eliminated in the preprocessing stage.

PLEASE, DISPLAY FIGURE 1 AROUND HERE

3. METHODOLOGY

In order to obtain the *ODI*3 of each of the study subjects, the total number of oxygen desaturations ≥ 3% from preceding SpO_2 baseline was divided by the total number of recording hours [12,19].

Then, we carried out a methodology in 3 stages. First, the AF bispectrum was estimated and 13 bispectral features were extracted to characterize it. Afterwards, a selection stage was applied using FCBF [33]. Finally, a MLP trained with the selected features was used to estimate the AHI.

3.1. Bispectrum estimation

Bispectrum is a high order spectrum (HOS) based on the 3rd order cumulant, i.e., on the spectral decomposition of skewness of time series histogram [12,26]. It is represented as the matrix that results of computing the 2-dimensional Fourier transform of the 3rd order cumulant of the signal by means of the following equation [12,26,34]:

$$B(f_x, f_y) = X(f_x) \cdot X(f_y) \cdot X^*(f_x + f_y), \qquad f_x, f_y = 0,..., f_N, \tag{1}$$

where f_x and f_y are the frequencies associated to the x and y axes of the bispectral matrix, f_N is the Nyquist frequency (sampling rate/2), $X(f)$ is the discrete Fourier transform (DFT), and each point (f_x, f_y) of the bispectral matrix indicates the phase coupling degree between frequency components [26].

As bispectrum preserves the amplitude and phase information, it is used to analyze interactions between patterns of a signal [12,26,28]. Moreover, bispectrum also allows to detect changes in the gaussianity of a time series [26,27]. In this regard, bispectral values

= 0 indicates that the signal components are normally distributed (gaussian components), while a bispectrum ≠ 0 indicate that the process have non-gaussian components [26]. In addition, bispectrum is able to detect deviations of linearity of a signal by means of the phase coupling between its frequency components [27,28]. The phase coupling between 3 harmonic components of frequencies f_1, f_2, and f_3 and phase angles ϕ_1, ϕ_2, and ϕ_3 is defined as $f_3 = f_1 + f_2$ and $\phi_3 = \phi_1 + \phi_2$ [26]. Thereby, the existence of phase coupling indicates that there are non-linear dependency relationships between harmonic components of the signal [26].

As bispectrum has symmetry properties, the computation of a triangular region is sufficient to completely describe it [26,27]. This area is known as the non-redundant computational region of the bispectrum and satisfies that $f_x \geq 0$, $f_y \geq f_x$, and $f_x + f_y \leq f_N$ [26]. Regarding the DFT computation, it implies the use of a temporal window that is moved along the signal to collect the frequency variation at each instant of time [35]. The window length is a parameter that affects the temporal and frequency resolution, so a compromise should be established between both resolutions [24]. In the case of pediatric OSA, apneic events last at least 2 respiratory cycles [3]. Therefore, a 30-s window length would assure that the segment contains sufficient frequency information about apneic events, without losing temporal resolution. Thus, a Hamming window of 2^{12} samples (≈ 30-s) with 50% overlap and 2^{13} points of DFT was used in our study to obtain the bispectrum.

Once the bispectrum was computed, it was normalized by dividing the bispectral matrix by the total bispectral power (*BP*) [26]:

$$B_N(f_x, f_y) = \frac{B(f_x, f_y)}{BP}, \qquad f_x, f_y = 0,..., f_N, \tag{2}$$

where *BP* is computed as the sum of all magnitudes of the complete bispectrum:

$$BP = \sum_{f_x, f_y=0}^{f_N} |B(f_x, f_y)|. \tag{3}$$

This normalization allows the magnitude values of the bispectrum to be between 0 and 1 [26], thus minimizing the inter-individual differences related to particular physiological features other than OSA [36]. Moreover, this normalization allows to measure the phase coupling degree between frequencies [26].

3.2. Feature extraction

It is well-known that the respiratory rate in children decreases from birth to adolescence [37]. Therefore, we used a bispectral band adapted to the respiratory rate of each child. In order to estimate it, we first located the pair of frequencies f_{xmax} and f_{ymax} for the maximum amplitude value of bispectrum. We located the point of maximum bispectral power, which corresponds to the peak of normal respiration. Afterwards, a bandwidth of 0.15 Hz was established [38,39]. Thereby, the resulting adaptive bispectral band (*AB*) for each subject was a square region of AF bispectrum defined by $f_x \in [f_{xmax} - 0.075\ \text{Hz}, f_{xmax} + 0.075\ \text{Hz}] \cap f_y \in [f_{ymax} - 0.075\ \text{Hz}, f_{ymax} + 0.075\ \text{Hz}]$.

Once the adaptive bispectral band (*AB*) was obtained from each of the 946 subjects, 13 bispectral features were extracted.

3.2.1. Features based on the amplitude of bispectral band

- Maximum amplitude (B_{max}). It is the maximum magnitude value located in the adaptive band [40]:

$$B_{\max} = \max(|B_N(f_x, f_y)|_{f_x, f_y \in AB}). \quad (4)$$

- Minimum amplitude (B_{min}). It is the minimum value of the bispectral band:

$$B_{\min} = \min(|B_N(f_x, f_y)|_{f_x, f_y \in AB}). \quad (5)$$

- Total power (B_{total}). This feature allows to measure the deviation of gaussianity [41]. B_{total} corresponds to the bispectral power of the adaptive band and it is obtained as the sum of magnitudes contained in this band [41]:

$$B_{total} = \sum_{f_x, f_y \in AB} | B_N(f_x, f_y) | . \quad (6)$$

Previous studies based on the spectral analysis of AF have shown that children without OSA concentrate higher spectral power close to normal respiratory band [14,18]. Similar to the spectral analysis, it was expected to find lower bispectral amplitudes and lower values of B_{max}, B_{min}, and B_{total} in the adaptive band of the subjects with OSA.

3.2.2. Features based on the entropy of bispectral distribution

- Bispectral entropies of first (BE_1), second (BE_2), and third (BE_3) order. These features measure the irregularity of the signal [12,26]. BE_1, BE_2, and BE_3 are calculated as the Shannon's entropy of the amplitude, the quadratic amplitude, and the cubic amplitude of the bispectral band, respectively [12,29]:

$$BE_i = -\sum_j p_j \cdot \log(p_j), \qquad j = 1,2,...,J , \quad (7)$$

where i is the order of entropy (i = 1, 2 or 3), J is the number of bins, and p is the distribution of amplitudes in the adaptive band:

$$p_j = \frac{| B_N(f_x, f_y) |^i}{\sum_{f_x, f_y \in AB} | B_N(f_x, f_y) |^i}, \qquad i = 1,2,3. \quad (8)$$

- Phase entropy (PE). PE quantifies the irregularity of the phase in the bispectral band [12]. Thereby, the Shannon's entropy is applied to the normalized distribution of the phase angles of this band [12,26]:

$$PE = -\sum_n p(\psi_n) \cdot \log[p(\psi_n)], \qquad n = 1,2,...,N , \quad (9)$$

where N is the number of bins and $p(\psi)$ is the distribution of the phase angles [12,26]:

$$p(\psi_n) = \frac{1}{L} \cdot \sum_{f_x, f_y \in AB} Ind[\phi(B_N(f_x, f_y)) \in \psi_n], \quad (10)$$

where L is the number of points of the adaptive band, ϕ is the phase angle, ψ is the range of histogram bins:

$$\psi_n = \left\{ \phi \left| -\pi + \frac{2 \cdot \pi \cdot n}{N} \le \phi < -\pi + \frac{2 \cdot \pi \cdot (n+1)}{N} \right. \right\}, \tag{11}$$

and $Ind[\cdot]$ is the indicator such that [26]:

$$Ind = \begin{cases} 1 : \phi(B_N(f_x, f_y)) \in \psi_n \\ 0 : otherwise \end{cases}. \tag{12}$$

It has been observed that AF signal presents higher irregularity in children with OSA [13,14]. Due to apneic events introduce variations of amplitude, phase, and frequency components in AF [13,14,18], higher values of BE_1, BE_2, BE_3, and PE are expected in presence of OSA.

3.2.3. Features based on the bispectral band moments

- Sum of logarithmic amplitudes (H_1), sum of logarithmic amplitudes of diagonal elements (H_2), and spectral moments of first and second order of amplitudes of diagonal elements (H_3 and H_4, respectively). These features allow to quantify the non-linearity of a signal and are calculated based on the amplitude values contained in the adaptive band (AB) and in its diagonal (AB_{diag}) [25,29]:

$$H_1 = \sum\nolimits_{f_x, f_y \in AB} \log(|\, B_N(f_x, f_y)\,|)\,. \tag{13}$$

$$H_2 = \sum\nolimits_{f_k \in AB_{diag}} \log(|\, B_N(f_k, f_k)\,|)\,. \tag{14}$$

$$H_3 = \sum\nolimits_{f_k \in AB_{diag}} k \cdot \log(|\, B_N(f_k, f_k)\,|)\,. \tag{15}$$

$$H_4 = \sum\nolimits_{f_k \in AB_{diag}} (k - H_3)^2 \cdot \log(|\, B_N(f_k, f_k)\,|)\,. \tag{16}$$

AF signals of children without OSA are expected to have their bispectral content more concentrated in the normal breathing band. This would imply greater phase coupling between the frequency components of this band and, therefore, greater non-linearity [29].

Consequently, higher values of H_1, H_2, H_3, and H_4 are expected in the subjects.

3.2.4. Features based on the weighted center of bispectrum (*WCOB*)

- *WCOB*. Bispectral weighted center is defined as an index to detect the focus of the adaptive band [27]. The weighted center in this band can be calculated by assigning a weight to each of its bispectral components [42]. Thus, *WCOB* is a 2-dimensional vector whose components are defined by [27,42]:

$$fm_1 = \frac{\sum_{f_x, f_y \in AB} f_x \cdot B_N(f_x, f_y)}{\sum_{f_x, f_y \in AB} B_N(f_x, f_y)}. \quad (17)$$

$$fm_2 = \frac{\sum_{f_x, f_y \in AB} f_y \cdot B_N(f_x, f_y)}{\sum_{f_x, f_y \in AB} B_N(f_x, f_y)}. \quad (18)$$

It provides a summary of the interaction between frequency components [42]. The *WCOB* values are related to the peaks of the bispectrum [42]. Particularly, a *WCOB* decrease (lower fm_1 and fm_2 values) is associated with activities in low frequency [42]. Thereby, subjects without OSA are expected to concentrate the bispectral content in the normal breathing band (higher bispectral peak). Consequently, it is expected that their *WCOB* is centered in this band, whereas in subjects with OSA it is shifted towards frequency components associated with apneic events.

3.3. Feature selection

The method used in this study to apply the selection stage was FCBF [33]. This algorithm has been widely used in the diagnosis of pediatric OSA [12,13,31,43]. Based on the symmetric uncertainty (*SU*) [33], FCBF allows to find an optimal subset of relevant and non-redundant features, thus reducing the high dimensionality and complexity of predictive models [44]. Moreover, it is a filter-type feature selection technique, so it provide results that do not depend on posterior analysis [44].

In order to obtain a stable and generalizable subset of features, FCBF was applied to 1000 bootstrap replicates from the training group [45]. The average significance, defined as the sum of the number of times the features are selected divided by the total number of input features, was used as threshold [32]. Therefore, the selected features (i.e. those that were relevant and non-redundant) a number of times equal or higher than the average significance constituted the optimal subset [32].

3.4. Apnea-hypopnea index estimation

AHI has been estimated by means of a MLP [46]. MLP uses the well-known backpropagation supervised learning technique for training and allows to distinguish data that is non-linearly separable [47,48]. MLP usually consists of three perceptron layers (input, hidden, and output), where each perceptron is connected with a certain weight to all the perceptrons of the next layer [46]. The number of perceptrons of the input layer is equal to the number of features that feed the network, while the number of perceptrons N_H of the hidden layer is a parameter to be tuned [46]. In our study, the output layer is formed by a single linear unit that estimates the AHI.

Weights were randomly initialized and then optimized by means of scaled conjugate gradient and weight decay [46]. The latter introduces a regularization parameter, α, to deal with overfitting [46]. Like N_H, α also requires to be tuned. In our study, both parameters were optimized by applying leave-one-out cross-validation (loo-cv) in the training group and computing the Cohen's kappa (k) for each N_H / α pair [12,31].

3.5. Statistical analysis

Bispectral features did not show normal distribution when Lilliefors test was applied. Hence, the non-parametric Kruskal-Wallis test was used to search for statistical significant differences (p-value < 0.01) among the four severity groups (no-OSA, mild,

moderate, and severe OSA). Moreover, the Mann-Whitney *U* test was used as *post-hoc* test for pairwise comparison between severity groups, applying the Bonferroni correction for multiple comparisons. In order to visualize these differences, as well as to analyze the distribution and tendencies of the bispectral features, violin plots were also obtained. Violin plots showed the data distribution of each extracted feature (black region), as well as the first quartile (lower red line), the median (middle red line), and the third quartile (upper red line) of the distribution. The agreement between the predicted and actual diagnosis was assessed using the four-class accuracy (Acc_4) and *k* [49]. The intra-class correlation coefficient (ICC) was also used to measure the agreement between the AHI estimated by the proposed models and the actual AHI from PSG. The metrics used to assess the diagnostic performance of the MLP were as follows: sensitivity (Se), specificity (Sp), accuracy (Acc), area under receiver-operating characteristic curve (AUC), and positive (LR+) and negative (LR-) likelihood ratios.

4. RESULTS

4.1. Training set

4.1.1. Descriptive analysis

Figure 2 shows the averaged normalized bispectrum by severity groups. Figure 3 displays the averaged adaptive bispectral band by severity groups in 3D. As can be seen, the bispectral information is distributed over a wider range of frequency components as the OSA severity degree increases. In the no-OSA group, the contour lines are more concentrated in the normal breathing band (yellow region at 0.20 Hz – 0.40 Hz in Figure 2). It is in this region where the no-OSA group presents higher averaged bispectral amplitude than the rest of the groups (0.017 Hz^{-1} according to Figure 3.a). However, the amplitude decreases in the normal breathing band and is distributed in a range of lower

frequencies (yellow region around 0.05 Hz in Figure 2) as the severity increases. Therefore, the subjects with greater severity show lower amplitude in the common respiration band while reaching higher amplitude ($\geq 2 \cdot 10^{-3}$ Hz^{-1}), and thus greater phase coupling, in a new frequency region around 0.05 Hz.

PLEASE, DISPLAY FIGURE 2 AND FIGURE 3 AROUND HERE

Figure 4 shows the violin plots of the 13 bispectral features extracted from the adaptive band and *ODI*3 of the 4 OSA severity groups in the training set. It can be observed that the features based on amplitude B_{max} and B_{total} experienced a decreasing tendency and different distribution as AHI increases. In contrast, B_{min} did not show a clear tendency or distribution differences between severity groups. BE_1, BE_2, BE_3, and *PE* showed similar distributions to each other and an increasing tendency with the rise of AHI. This tendency was clearer in BE_1. The features based on moments (H_1, H_2, H_3, and H_4) presented similar distributions, as well as a decreasing tendency as the severity of OSA increases. Regarding the *WCOB*-based features, fm_1 and fm_2 showed different distribution to each other and among severity groups. While fm_1 experienced a slight increasing tendency, it was decreasing for fm_2. It can also be noted that *ODI*3 presented an increasing tendency with the increase of OSA severity. However, it did not show distribution differences between severity groups.

PLEASE, DISPLAY FIGURE 4 AROUND HERE

Of the 13 extracted bispectral features, all except B_{min} and fm_1 showed statistically significant differences (p-value < 0.01) among the 4 OSA severity groups when the Kruskal-Wallis test was applied. With the Mann-Whitney *U* test, no differences were found between the no-OSA and mild OSA group in any bispectral feature. However, all the features but B_{min} and fm_1, reflected differences between the severe OSA group and the

other groups. Statistically significant differences in B_{max}, B_{total}, H_2, and H_4 were also found between the no-OSA and moderate OSA group, and only B_{total} showed differences between the mild OSA and moderate OSA group. Regarding *ODI*3, it presented statistically significant differences in all comparisons between OSA severity groups.

4.1.2. Features selected by FCBF

Figure 5 displays the histograms of the number of times each feature was selected using FCBF in 1000 bootstrap replicates from the training set. Results of feature selection without *ODI*3 are shown in Figure 5.a. In this case, 4 bispectral features were selected as relevant and non-redundant more times than the average significance: B_{min}, BE_1, H_2, and fm_2. Moreover, results of feature selection with *ODI*3 are shown in Figure 5.b. It can be seen that BE_1, H_2, fm_2, and *ODI*3 formed the optimal feature subset.

PLEASE, DISPLAY FIGURE 5 AROUND HERE

Figure 6 shows the heat map of the *SU* between each pair of features x_i and x_j ($SU(x_i|x_j)$). Each region of this map was computed as the median of the $SU(x_i|x_j)$ obtained in the 1000 bootstrap replicates. As can be observed, $SU(x_i|x_j)$ values vary between 0 and 1 according to the redundancy degree, where a $SU(x_i|x_j) = 1$ means that one feature is completely predictable from the other and a $SU(x_i|x_j) = 0$ indicates that the two features are independent. In this regard, high $SU(x_i|x_j)$ was presented between the bispectral features from the same approach: features based on bispectral entropies, moments, and *WCOB*. The features based on amplitude B_{max} and B_{total} also showed high $SU(x_i|x_j)$ with each other, as well as with features from other bispectral approaches (B_{max} with bispectral entropies and B_{total} with features based on moments). In contrast, the $SU(x_i|x_j)$ of $B_{\min}$, *PE*, and *ODI*3 with the rest of features was lower.

PLEASE, DISPLAY FIGURE 6 AROUND HERE

4.1.3. Optimization and training of MLP

We trained a MLP model for each of the 2 optimal subsets that were obtained in the selection stage: MLP^{AF} (MLP input: B_{min}, BE_1, H_2, and fm_2) and $MLP^{AF,ODI3}$ (MLP input: BE_1, H_2, fm_2, and *ODI*3). In order to optimize N_H and α, we varied their values from 1 to 40 and from 1 to 20 in steps of 1, respectively. For each N_H / α pair, k was obtained through a loo-cv procedure in the training group. The maximum value of k determined the optimal values of N_H and α in each case. Thereby, the optimal values of MLP^{AF} were $N_H = 39$ and $\alpha = 7$, while the optimal values of $MLP^{AF,ODI3}$ were $N_H = 2$ and $\alpha = 8$. Finally, MLP^{AF} and $MLP^{AF,ODI3}$ networks, configured with the optimized parameters, were trained with the entire training group to complete the learning process.

4.2. Test set

The trained MLP^{AF}, $MLP^{AF,ODI3}$ networks, as well as single *ODI*3 were assessed using the test group. In this way, the 3 models were applied to 1000 bootstrap replicates derived from the test group while the performance metrics were obtained for each replicate using the bootstrap 0.632 procedure [45]. The median and the 95% confidence interval of all performance metrics were computed. Statistical differences between each pair of models were assessed using the Mann-Whitney *U* test with the Bonferroni correction. The evaluation results are shown in Table 2 and Table 3.

PLEASE, DISPLAY TABLE 2 AND TABLE 3 AROUND HERE

Despite the moderate diagnostic performance obtained by MLP^{AF}, it significantly outperformed *ODI*3 (p-value < 0.001) in Se for 1 and 5 events/h, and in Acc for 1 event/h. It can be seen that MLP^{AF} overestimates the OSA severity degree in 1 and 5 events/h, while *ODI*3 underestimates it. However, this effect is reduced when the 2 approaches (bispectral features from AF and *ODI*3) are combined in $MLP^{AF,ODI3}$, thus reflecting the

complementarity of both approaches. This model achieved significantly higher diagnostic accuracy (p-value < 0.001) than the 2 approaches separately for the 3 cut-off points. It is also noticeable the value of LR+ = 15.01 [11.82 - 30.73] achieved by $MLP^{AF,ODI3}$ for 10 events/h. Regarding the global performance measures (Table 3), the $MLP^{AF,ODI3}$ also significantly outperformed MLP^{AF} and single *ODI*3 (p-value < 0.001) in terms of k and Acc_4.

5. DISCUSSION

In this study, we characterized the non-gaussianity, non-linearity, and irregularity of AF signal through bispectrum, and extracted previously uncovered features in the childhood OSA context. Moreover, our study highlighted the complementarity among the 4 bispectral approaches applied to AF, as well as the complementarity between the bispectral information from AF and the commonly employed index *ODI*3. Finally, we evaluated its performance to diagnose OSA in children. These computational findings allowed for development of a MLP model with high diagnostic accuracy whenever using any of the common clinical cut-offs for OSA severity, namely 1, 5, and 10 events/h (82.16% [79.83 – 84.44], 82.49% [80.08 – 84.77], and 90.15% [88.39 – 92.00], respectively) by combining bispectral features from AF and *ODI*3. The interpretation of these novel results is detailed below.

5.1. Selected features

The averaged normalized bispectrum (Figure 2) reflected the degree of phase coupling between different frequency components. In this regard, it was observed that the subjects without OSA presented a strong coupling in the normal respiration frequency range (0.20 Hz - 0.40 Hz). However, the subjects with OSA showed a redistribution of the bispectral power, with a decrease of amplitude and coupling in their adaptive band

(Figure 3). This decrease suggest that apneic events reduce the non-gaussianity and the non-linearity of AF signal [26].

These changes of amplitude and coupling were also quantified by means of the extracted bispectral features. In this regard, FCBF revealed the relevance and complementarity of B_{min}, BE_1, H_2, and fm_2, as well as the redundancy of the remaining extracted information (Figure 5.a and Figure 6). Since the bispectrum from AF is normalized, minimum amplitude (B_{min}) allowed to estimate the minimum coupling generated within the adaptive band. Although this feature did not show statistical differences between the OSA severity groups (Figure 4), it provides complementary information focused on strength of minimum coupling instead of irregularity or coupling focus localization of AF.

Moreover, bispectral entropy of first order (BE_1) showed an increasing tendency as AHI was higher (Figure 4), which implies an increase of irregularity in the amplitude of AF signal [12,26]. Hence, this increase suggests that apneic events generate a loss in the synchronization of the respiratory rhythm, causing AF to abruptly change its amplitude without following a determined pattern [29].

Regarding the sum of logarithmic amplitudes of diagonal elements of the bispectral band (H_2), it experienced a decreasing tendency as OSA severity degree increased (Figure 4). Since the frequency components of the diagonal are $f_1 = f_2$, this feature provides information about the phase coupling between the harmonic components of AF, such that $f_3 = 2 \cdot f_1$ and $\phi_3 = 2 \cdot \phi_1$ [29,34]. Therefore, its decreasing tendency would indicate less non-linear interaction between the AF harmonic components of subjects with OSA. This fact suggests that the occurrence of apneic events generates less periodic and more random harmonic components in the AF signal [29,34].

In addition, fm_2 revealed that OSA introduces changes in the location of the focus of bispectral band coupling. In this regard, the less severe groups presented the coordinate *y* of their weighted centers (fm_2) more concentrated within the central region of the bispectral band (Figure 4). The decreasing tendency of this feature suggests that apneas and hypopneas displace the coupling focus, generating more activity in the low frequency components of the adaptive band [42].

According to Figure 6, it was observed that bispectral features from the same approach (features based on amplitude, entropies, moments, and *WCOB*) share a large amount of information with each other (high $SU(x_i|x_j)$). This supported the fact that FCBF only selected one feature from each of the 4 bispectral approaches (Figure 5.a), hence highlighting the existing complementarity among them. When *ODI*3 was included in the process, it was selected along with BE_1, H_2, and fm_2 (Figure 5.b). This fact revealed that the information provided by bispectrum about the irregularity, non-linearity, and coupling focus from AF is consistent and complementary to that provided by *ODI*3.

5.2. Diagnostic performance

The complementarity between the bispectral information from AF and *ODI*3 was also reflected in the MLP models used to estimate the AHI. The $MLP^{AF,ODI3}$ model showed a statistically significant higher performance (*p*-value < 0.001) in terms of Se, Acc, and LR- for 1 and 5 events/h, in Sp, Acc, AUC, and LR+ for 10 events/h, as well as in *k* and Acc_4. $MLP^{AF,ODI3}$ obtained higher performance than MLP^{AF} and *ODI*3 in the global measures *k* and Acc_4, revealing that the agreement between the predicted and actual severity is greater when both approaches are jointly used. In this regard, MLP^{AF} showed an overestimation of OSA (low Sp values) in 1 and 5 events/h, while *ODI*3 showed an underestimation (low Se values) in these cut-off points. In contrast, the combination of both approaches in $MLP^{AF,ODI3}$ reduced this effect in 5 events/h. Although

$MLP^{AF,ODI3}$ obtained an unbalanced Se-Sp pair in 1 event/h, this model achieved high performance in the global diagnostic measurement (AUC = 0.82 [0.79 – 0.84]).

Moreover, the complementarity of both approaches could also be observed in the diagnostic accuracy. While MLP^{AF} and *ODI*3 reached moderate diagnostic accuracies in 1, 5, and 10 events/h, $MLP^{AF,ODI3}$ achieved statistically significant higher accuracy (*p*-value < 0.001) in these 3 cut-off points (82.16% [79.83 – 84.44], 82.49% [80.08 – 84.77], and 90.15% [88.39 – 92.00], respectively), improving those individually obtained by each of the approaches. In addition, it is also remarkable the significant increase in LR+ (*p*-value < 0.001) reached by $MLP^{AF,ODI3}$ for 10 events/h (LR+ = 15.01 [11.82 - 30.73]). Due to a LR+ ≥ 10 is a robust indicator to confirm the presence of a disease [50], this model could be applied to early detect severe OSA cases. Accordingly, our proposal could be very useful to simplify the pediatric OSA diagnosis, particularly for those children with moderate-to-severe OSA. These subjects have an increased risk of developing neurocognitive and cardiovascular comorbidities [1,2,30]. Thus, our proposal would not only serve to streamline long waiting lists, but also to quickly diagnose children before the adverse consequences of OSA continue progressing and potentially become irreversible. Moreover, it could help to reduce the complexity and intrusiveness of pediatric OSA diagnostic tests, such as PSG and HRP.

5.3. Comparison with other studies

Table 4 summarizes the results achieved in previous studies focused on OSA detection in children [8,9,12–14,31,43,51–53]. Several of these studies evaluated their methodologies involving a low-to-moderate number of pediatric subjects (whole dataset ranging from 21 to 298 children, with test set ranging from 21 to 207 subjects) [8,9,12,51–53]. These studies reported Acc ranging from 75.00% to 84.00% and AUC ranging from 0.80 to 0.86 for 1 event/h, 71.00% to 85.10% Acc and 0.78 to 0.91 AUC for 5 events/h,

and 85.33% to 89.00% Acc and 0.92 to 0.94 AUC for 10 events/h. Our proposal was designed and assessed using 946 children (376 subjects in the test set) and achieved performances close to the maximum values of these ranges, including the maximum Acc value for 10 events/h.

PLEASE, DISPLAY TABLE 4 AROUND HERE

Other studies have already assessed their approaches with larger number of subjects (whole dataset ranging from 432 to 4191 children, with test set ranging from 251 to 3602 individuals) [14,15,31,43]. These studies achieved a high diagnostic performance for 1, 5, and 10 events/h. However, our methodology obtained higher diagnostic accuracy in 1 and 5 events/h, similar Acc in 10 events/h (90.26%), as well as higher AUC in the 3 cut-off points.

A previous study from our research group analyzed the AF signal in the pediatric OSA context using recurrence plots (RPs) [13]. Beyond the further characterization obtained by means of bispectrum, we have been able to notably improve the reported diagnostic performance for 5 events/h. As moderately to severely affected children have an increased risk of developing comorbidities [1,2,30], this improvement impacts on those children who benefit the most from an early diagnosis and a timely treatment. Moreover, adenotonsillectomy is commonly recommended when pediatric subjects present an AHI $\geq$ 5 events/h [1,2]. Thus, bispectrum could be more useful than RPs to diagnose these cases on time. In addition to the improvement in 5 events/h, our current proposal obtained a slightly lower performance to discard OSA (LR- = 0.14 vs. LR- = 0.10 for 1 event/h) and a higher performance to confirm the presence of severe OSA (LR+ = 15.01 vs. LR+ = 13.71 for 10 events/h) than the method based on RPs. Thereby, bispectrum would be a more robust method detecting cases of pediatric severe OSA. It should also be noted that the bispectral analysis has revealed behaviors of AF, such as

changes of gaussianity and linearity, that could not have been detected by means of RPs. Another study from our group analyzed the bispectrum from SpO_2 signal along with *ODI*3, anthropometric, and spectral features to classify children in 3 OSA severity groups [12]. However, our AHI estimation using the bispectral information from AF and *ODI*3 outperformed its results. Hence, our proposal has shown a high diagnostic performance compared to other state-of-the-art studies.

5.4. Limitations

Several limitations of our study need to be pointed out. The database used in this study was formed by 946 pediatric subjects. Although this sample is large, it would be desirable that the size of the severity groups had been more balanced. However, the proportion of subjects is similar to that reflected by other state-of-the-art studies in the context of detection of pediatric OSA [31,43,52,53]. In addition, although some studies indicate that respiratory rate varies with age, there is no consensus on which their reference ranges are [37]. Regarding bispectral bandwidth, we used a width of 0.15 Hz, like some studies based on spectral analysis that involved the respiratory rate of children [38,39]. However, different frequency ranges of the bispectrum could be analyzed in future studies, and even bandwidth could also be considered an adaptive factor. Moreover, AHI could be estimated using other techniques, such as ensemble-learning methods, or multiclass classifiers, and the results obtained with each of them could be compared in future research.

6. CONCLUSION

As far as we know, this is the first time that bispectrum is used to characterize AF in the pediatric OSA context. We found that the occurrence of apneic events decreases the non-gaussianity and the non-linear interaction of the harmonic components of AF

signal, as well as the regularity of the respiratory patterns. Another contribution of this study is the use of a bispectral band adapted to the physiological conditions of each subject. Our results revealed that the different approaches of bispectral features extracted from this band (features based on amplitude, entropies, moments, and *WCOB*) provide complementary information to characterize AF in children. In addition, we found that the bispectrum from AF provides complementary information to *ODI*3, improving the performance individually achieved by each of these approaches. Therefore, the MLP model fed with bispectral features and *ODI*3 reached high diagnostic performance in discriminating moderately to severely affected children. These results lead us to conclude that the information provided by bispectrum is able to characterize pediatric OSA from AF signals. Thus, bispectral information from AF and *ODI*3 could be jointly used as a simplified methodology to improve the automated OSA diagnosis in children.

ACKNOWLEDGEMENTS

This work was supported by 'Ministerio de Ciencia, Innovación y Universidades' and ‘European Regional Development Fund (FEDER)’ under projects DPI2017-84280-R and RTC-2017-6516-1, and by ‘CIBER en Bioingeniería, Biomateriales y Nanomedicina (CIBER-BBN)’ through ‘Instituto de Salud Carlos III’ co-funded with FEDER funds. Verónica Barroso-García was in receipt of a ‘Ayuda para financiar la contratación predoctoral de personal investigador’ grant from ‘Consejería de Educación de la Junta de Castilla y León’ cofunded by ‘European Social Fund’. Fernando Vaquerizo-Villar was in receipt of a ‘Ayuda para contratos predoctorales para la Formación de Profesorado Universitario (FPU)’ grant from ‘Ministerio de Educación, Cultura y Deporte’ (FPU16/02938). Leila Kheirandish-Gozal and David Gozal are supported by ‘National Institutes of Health (NIH)’ grants HL130984, HL140548, and AG061824.

CONFLICT OF INTEREST STATEMENT

There are no conflicts of interest that could inappropriately influence this research work.

ETHICAL APPROVAL

This work has been carried out according to the Declaration of Helsinki. The informed consents of all children caretakers were obtained, and the Ethics Committee of the Comer Children's Hospital approved the protocol of the study (#11-0268-AM017, #09-115-B-AM031, and #IRB14-1241).

AUTHORSHIP CONTRIBUTION STATEMENT

Data collection: L. Kheirandish-Gozal and D. Gozal; Medical diagnostic: L. Kheirandish-Gozal and D. Gozal; Study design: G.C. Gutiérrez-Tobal, L. Kheirandish-Gozal, D. Gozal, and R. Hornero; Signal processing: V. Barroso-García; Data analysis: V. Barroso-García; Results interpretation: V. Barroso-García, G.C. Gutiérrez-Tobal, F. Vaquerizo-Villar, D. Álvarez, F. del Campo, and R. Hornero. Writing - original draft: V. Barroso-García; Writing - review and editing: V. Barroso-García, G.C. Gutiérrez-Tobal, F. Vaquerizo-Villar, D. Álvarez, D. Gozal, and R. Hornero. All authors gave their final approval of this version of the manuscript.

REFERENCES

[1] A.G. Kaditis, M.L.A. Alvarez, A. Boudewyns, E.I. Alexopoulos, R. Ersu, K. Joosten, H. Larramona, S. Miano, I. Narang, H. Trang, M. Tsaoussoglou, N. Vandenbussche, M.P. Villa, D. Van Waardenburg, S. Weber, S. Verhulst,

Obstructive sleep disordered breathing in 2- to 18-year-old children: Diagnosis and management, Eur. Respir. J. 47 (2016) 69–94. doi:10.1183/13993003.00385-2015.

[2] M. Luz Alonso-Álvarez, T. Canet, M. Cubell-Alarco, E. Estivill, E. Fernández-Julián, D. Gozal, M.J. Jurado-Luque, M.A. Lluch-Roselló, F. Martínez-Pérez, M. Merino-Andreu, G. Pin-Arboledas, N. Roure, F.X. Sanmartí, Ó. Sans-Capdevila, F. Segarra-Isern, M. Tomás-Vila, J. Terán-Santos, Consensus document on sleep apnea-hypopnea syndrome in children, Arch. Bronconeumol. 47 (2011) 2–18. doi:10.1016/S0300-2896(11)70026-6.

[3] R.B. Berry, R. Budhiraja, D.J. Gottlieb, D. Gozal, C. Iber, V.K. Kapur, C.L. Marcus, R. Mehra, S. Parthasarathy, S.F. Quan, S. Redline, K.P. Strohl, S.L.D. Ward, M.M. Tangredi, Rules for Scoring Respiratory Events in Sleep: Update of the 2007 AASM Manual for the Scoring of Sleep and Associated Events, J. Clin. Sleep Med. 08 (2012) 597–619. doi:10.5664/jcsm.2172.

[4] C. Jon, Polysomnography in Children, in: Pediatr. Otolaryngol. Clin., Humana Press, Totowa, NJ, 2009: pp. 35–47. doi:10.1007/978-1-60327-127-1_5.

[5] K. Spruyt, Pediatric Sleep-Disordered Breathing: Criteria and Spectrum of Disease, in: L. Kheirandish-Gozal, D. Gozal (Eds.), Sleep Disord. Breath. Child., Humana Press, New York, 2012: pp. 245–60. doi:10.1007/978-1-60761-725-9_18.

[6] P.J. Ryan, M.F. Hilton, D.A. Boldy, A. Evans, S. Bradbury, S. Sapiano, K. Prowse, R.M. Cayton, Validation of British Thoracic Society guidelines for the diagnosis of the sleep apnoea/hypopnoea syndrome: can polysomnography be avoided?, Thorax. 50 (1995) 972–975. doi:10.1136/thx.50.9.972.

[7] E. Chiner, C. Cánovas, V. Molina, J.N. Sancho-Chust, S. Vañes, E. Pastor, M.A. Martinez-Garcia, Home Respiratory Polygraphy is Useful in the Diagnosis of Childhood Obstructive Sleep Apnea Syndrome, J. Clin. Med. 9 (2020) 2067.

doi:10.3390/jcm9072067.

[8] R.B. Shouldice, L.M. O'Brien, C. O'Brien, P. de Chazal, D. Gozal, C. Heneghan, Detection of Obstructive Sleep Apnea in Pediatric Subjects using Surface Lead Electrocardiogram Features, Sleep. 27 (2004) 784–92. doi:10.1093/sleep/27.4.784.

[9] E. Gil, R. Bailon, J.M. Vergara, P. Laguna, PTT Variability for Discrimination of Sleep Apnea Related Decreases in the Amplitude Fluctuations of PPG Signal in Children, IEEE Trans. Biomed. Eng. 57 (2010) 1079–88. doi:10.1109/tbme.2009.2037734.

[10] J. Lazaro, E. Gil, J.M. Vergara, P. Laguna, Pulse Rate Variability Analysis for Discrimination of Sleep-Apnea-Related Decreases in the Amplitude Fluctuations of Pulse Photoplethysmographic Signal in Children, IEEE J. Biomed. Heal. Informatics. 18 (2014) 240–6. doi:10.1109/JBHI.2013.2267096.

[11] A. Garde, P. Dehkordi, W. Karlen, D. Wensley, J.M. Ansermino, G.A. Dumont, Development of a Screening Tool for Sleep Disordered Breathing in Children Using the Phone Oximeter™, PLoS One. 9 (2014) e112959. doi:10.1371/journal.pone.0112959.

[12] F. Vaquerizo-Villar, D. Álvarez, L. Kheirandish-Gozal, G.C. Gutiérrez-Tobal, V. Barroso-García, A. Crespo, F. del Campo, D. Gozal, R. Hornero, Utility of bispectrum in the screening of pediatric sleep apnea-hypopnea syndrome using oximetry recordings, Comput. Methods Programs Biomed. 156 (2018) 141–149. doi:10.1016/J.CMPB.2017.12.020.

[13] V. Barroso-García, G.C. Gutiérrez-Tobal, L. Kheirandish-Gozal, D. Álvarez, F. Vaquerizo-Villar, P. Núñez, F. del Campo, D. Gozal, R. Hornero, Usefulness of recurrence plots from airflow recordings to aid in paediatric sleep apnoea

diagnosis, Comput. Methods Programs Biomed. 183 (2020) 105083. doi:10.1016/j.cmpb.2019.105083.

[14] V. Barroso-García, G. Gutiérrez-Tobal, L. Kheirandish-Gozal, D. Álvarez, F. Vaquerizo-Villar, A. Crespo, F. del Campo, D. Gozal, R. Hornero, Irregularity and Variability Analysis of Airflow Recordings to Facilitate the Diagnosis of Paediatric Sleep Apnoea-Hypopnoea Syndrome, Entropy. 19 (2017) 447. doi:10.3390/e19090447.

[15] J. Jiménez-García, G.C. Gutiérrez-Tobal, M. García, L. Kheirandish-Gozal, A. Martín-Montero, D. Álvarez, F. del Campo, D. Gozal, R. Hornero, Assessment of Airflow and Oximetry Signals to Detect Pediatric Sleep Apnea-Hypopnea Syndrome Using AdaBoost, Entropy. 22 (2020) 670. doi:10.3390/e22060670.

[16] N.A. Collop, W.M.D. Anderson, B. Boehlecke, D. Claman, R. Goldberg, D.J. Gottlieb, D. Hudgel, M. Sateia, R. Schwab, Clinical guidelines for the use of unattended portable monitors in the diagnosis of obstructive sleep apnea in adult patients, J. Clin. Sleep Med. 3 (2007) 737–747. doi:10.5664/jcsm.27032.

[17] F. Stehling, J. Keull, M. Olivier, J. Große-Onnebrink, U. Mellies, B.A. Stuck, Validation of the screening tool ApneaLink® in comparison to polysomnography for the diagnosis of sleep-disordered breathing in children and adolescents, Sleep Med. 37 (2017) 13–18. doi:10.1016/j.sleep.2017.05.018.

[18] G.C. Gutiérrez-Tobal, M.L. Alonso-Álvarez, D. Álvarez, F. del Campo, J. Terán-Santos, R. Hornero, Diagnosis of pediatric obstructive sleep apnea: Preliminary findings using automatic analysis of airflow and oximetry recordings obtained at patients' home, Biomed. Signal Process. Control. 18 (2015) 401–7. doi:10.1016/j.bspc.2015.02.014.

[19] B.H. Taha, J.A. Dempsey, S.M. Weber, M.S. Badr, J.B. Skatrud, T.B.. Young, A.J.

Jacques, K.C. Seow, Automated detection and classification of sleep-disordered breathing from conventional polysomnography data, Sleep. 20 (1997) 991–1001. doi:10.1093/sleep/20.11.991.

[20] A. Kaditis, L. Kheirandish-Gozal, D. Gozal, Pediatric OSAS: Oximetry can provide answers when polysomnography is not available, Sleep Med. Rev. 27 (2015) 96–105. doi:10.1016/j.smrv.2015.05.008.

[21] B. Oeverland, O. Skatvedt, K.J. Kvarner, H. Akre, Pulseoximetry: Sufficient to diagnose severe sleep apnea, Sleep Med. 3 (2002) 133–138. doi:10.1016/S1389-9457(01)00122-8.

[22] V.G. Kirk, S.G. Bohn, W.W. Flemons, J.E. Remmers, Comparison of Home Oximetry Monitoring with Laboratory Polysomnography in Children, Chest. 124 (2003) 1702–1708. doi:10.1378/chest.124.5.1702.

[23] G.C. Gutierrez-Tobal, R. Hornero, D. Álvarez, J.V. Marcos, F. del Campo, Linear and nonlinear analysis of airflow recordings to help in sleep apnoea–hypopnoea syndrome diagnosis, Physiol. Meas. 33 (2012) 1261–75. doi:10.1088/0967-3334/33/7/1261.

[24] S. Pola, A. Macerata, M. Emdin, C. Marchesi, Estimation of the power spectral density in nonstationary cardiovascular time series: Assessing the role of the time-frequency representations (TFR), IEEE Trans. Biomed. Eng. 43 (1996) 46–59. doi:10.1109/10.477700.

[25] S.M. Zhou, J.Q. Gan, F. Sepulveda, Classifying mental tasks based on features of higher-order statistics from EEG signals in brain-computer interface, Inf. Sci. (Ny). 178 (2008) 1629–1640. doi:10.1016/j.ins.2007.11.012.

[26] K.C. Chua, V. Chandran, U.R. Acharya, C.M. Lim, Application of higher order statistics/spectra in biomedical signals-A review, Med. Eng. Phys. 32 (2010) 679–

689. doi:10.1016/j.medengphy.2010.04.009.

[27] J.W. Zhang, C.X. Zheng, A. Xie, Bispectrum analysis of focal ischemic cerebral EEG signal using third-order recursion method, IEEE Trans. Biomed. Eng. 47 (2000) 352–359. doi:10.1109/10.827296.

[28] M. Emin Tagluk, N. Sezgin, A new approach for estimation of obstructive sleep apnea syndrome, Expert Syst. Appl. 38 (2011) 5346–5351. doi:10.1016/j.eswa.2010.10.022.

[29] R. Atri, M. Mohebbi, Obstructive sleep apnea detection using spectrum and bispectrum analysis of single-lead ECG signal, Physiol. Meas. 36 (2015) 1963–1980. doi:10.1088/0967-3334/36/9/1963.

[30] G.D. Church, The Role of Polysomnography in Diagnosing and Treating Obstructive Sleep Apnea in Pediatric Patients, Curr. Probl. Pediatr. Adolesc. Health Care. 42 (2012) 2–25. doi:10.1016/J.CPPEDS.2011.10.001.

[31] R. Hornero, L. Kheirandish-Gozal, G.C. Gutiérrez-Tobal, M.F. Philby, M.L. Alonso-Álvarez, D. Álvarez, E.A. Dayyat, Z. Xu, Y.-S. Huang, M. Tamae Kakazu, A.M. Li, A. Van Eyck, P.E. Brockmann, Z. Ehsan, N. Simakajornboon, A.G. Kaditis, F. Vaquerizo-Villar, A. Crespo Sedano, O. Sans Capdevila, M. von Lukowicz, J. Terán-Santos, F. Del Campo, C.F. Poets, R. Ferreira, K. Bertran, Y. Zhang, J. Schuen, S. Verhulst, D. Gozal, Nocturnal Oximetry-based Evaluation of Habitually Snoring Children., Am. J. Respir. Crit. Care Med. 196 (2017) 1591–1598. doi:10.1164/rccm.201705-0930OC.

[32] D. Álvarez, A. Cerezo-Hernández, A. Crespo, G.C. Gutiérrez-Tobal, F. Vaquerizo-Villar, V. Barroso-García, F. Moreno, C.A. Arroyo, T. Ruiz, R. Hornero, F. del Campo, A machine learning-based test for adult sleep apnoea screening at home using oximetry and airflow, Sci. Rep. 10 (2020) 5332. doi:10.1038/s41598-020-

62223-4.

[33] L. Yu, Liu, Efficient Feature Selection via Analysis of Relevance and Redundancy, J. Mach. Learn. Res. 5 (2004) 1205–24.

[34] S. Marceglia, A.M. Bianchi, G. Baselli, G. Foffani, F. Cogiamanian, N. Modugno, S. Mrakic-Sposta, A. Priori, S. Cerutti, Interaction between rhythms in the human basal ganglia: Application of bispectral analysis to local field potentials, IEEE Trans. Neural Syst. Rehabil. Eng. 15 (2007) 483–492. doi:10.1109/TNSRE.2007.907893.

[35] L. Sörnmo, P. Laguna, Bioelectrical Signal Processing in Cardiac and Neurological Applications, 1st ed., Elsevier Inc., 2005. doi:10.1016/B978-0-12-437552-9.X5000-4.

[36] M.R. Nuwer, Quantitative EEG: I. techniques and problems of frequency analysis and topographic mapping, J. Clin. Neurophysiol. 5 (1988) 1–44. doi:10.1097/00004691-198801000-00001.

[37] S. Fleming, M. Thompson, R. Stevens, C. Heneghan, A. Plüddemann, I. MacOnochie, L. Tarassenko, D. Mant, Normal ranges of heart rate and respiratory rate in children from birth to 18 years of age: A systematic review of observational studies, Lancet. 377 (2011) 1011–1018. doi:10.1016/S0140-6736(10)62226-X.

[38] J. Milagro, E. Gil, J. Lazaro, V.P. Seppa, L. Pekka Malmberg, A.S. Pelkonen, A. Kotaniemi-Syrjanen, M.J. Makela, J. Viik, R. Bailon, Nocturnal Heart Rate Variability Spectrum Characterization in Preschool Children with Asthmatic Symptoms, IEEE J. Biomed. Heal. Informatics. 22 (2018) 1332–1340. doi:10.1109/JBHI.2017.2775059.

[39] J. Milagro, J. Gracia, V.-P. Seppa, J. Karjalainen, M. Paassilta, M. Orini, R. Bailon, E. Gil, J. Viik, Noninvasive Cardiorespiratory Signals Analysis for Asthma

Evolution Monitoring in Preschool Children, IEEE Trans. Biomed. Eng. (2019) 1–1. doi:10.1109/tbme.2019.2949873.

[40] Y. Wang, W. Wang, Y. Liu, D. Wang, B. Liu, Y. Shi, P. Gao, Feature extracting of weak signal in real-time sleeping EEG with approximate entropy and bispectrum analysis, in: 3rd Int. Conf. Bioinforma. Biomed. Eng. ICBBE 2009, IEEE, 2009: pp. 1–4. doi:10.1109/ICBBE.2009.5162854.

[41] T. Ning, J.D. Bronzino, Autoregressive and Bispectral Analysis Techniques: EEG Applications, IEEE Eng. Med. Biol. Mag. 9 (1990) 47–50. doi:10.1109/51.62905.

[42] R. Wang, J. Wang, S. Li, H. Yu, B. Deng, X. Wei, Multiple feature extraction and classification of electroencephalograph signal for Alzheimers' with spectrum and bispectrum, Chaos. 25 (2014) 013110. doi:10.1063/1.4906038.

[43] Z. Xu, G.C. Gutiérrez-Tobal, Y. Wu, L. Kheirandish-Gozal, X. Ni, R. Hornero, D. Gozal, Cloud Algorithm-Driven Oximetry-Based Diagnosis of Obstructive Sleep Apnea in Symptomatic Habitually-Snoring Children., Eur. Respir. J. (2018) 1801788. doi:10.1183/13993003.01788-2018.

[44] I. Guyon, An Introduction to Variable and Feature Selection, J. Mach. Learn. Res. 3 (2003) 1157–1182.

[45] I.H. Witten, E. Frank, M.A. Hall, Data mining: practical machine learning tools and techniques, Third, Morgan Kaufmann/Elsevier, Burlington, 2011. doi:10.1016/C2009-0-19715-5.

[46] C.M. Bishop, Neural networks for pattern recognition, Oxford university Press, 1996.

[47] D.E. Rumelhart, G.E. Hinton, R.J. Williams, Learning internal representations by error propagation, 1985.

[48] G. Cybenko, Approximation by superpositions of a sigmoidal function, Math.

Control. Signals, Syst. 2 (1989) 303–314. doi:10.1007/BF02551274.

[49] J. Cohen, A Coefficient of Agreement for Nominal Scales, Educ. Psychol. Meas. 20 (1960) 37–46. doi:10.1177/001316446002000104.

[50] J.J. Deeks, D.G. Altman, Diagnostic tests 4: likelihood ratios, BMJ. 329 (2004) 168–9. doi:10.1136/bmj.329.7458.168.

[51] P. Dehkordi, A. Garde, W. Karlen, C.L. Petersen, D. Wensley, G.A. Dumont, J. Mark Ansermino, Evaluation of cardiac modulation in children in response to apnea/hypopnea using the Phone Oximeter ™, Physiol. Meas. 37 (2016) 187–202. doi:10.1088/0967-3334/37/2/187.

[52] C.-M. Tsai, C.-H. Kang, M.-C. Su, H.-C. Lin, E.-Y. Huang, C.-C. Chen, J.-C. Hung, C.-K. Niu, D.-L. Liao, H.-R. Yu, Usefulness of desaturation index for the assessment of obstructive sleep apnea syndrome in children, Int. J. Pediatr. Otorhinolaryngol. 77 (2013) 1286–90. doi:10.1016/J.IJPORL.2013.05.011.

[53] A. Garde, X. Hoppenbrouwer, P. Dehkordi, G. Zhou, A.U. Rollinson, D. Wensley, G.A. Dumont, J.M. Ansermino, Pediatric pulse oximetry-based OSA screening at different thresholds of the apnea-hypopnea index with an expression of uncertainty for inconclusive classifications, Sleep Med. 60 (2019) 45–52. doi:10.1016/j.sleep.2018.08.027.

TABLES:

	All	Training set	Test set
Subjects (*n*)	946	570	376
Age (years)	6 [6]	6 [5]	6 [6]
Males (*n*)	584 (61.7%)	339 (59.5%)	245 (65.2%)
BMI (kg/m^2)	17.9 [6.2]	17.7 [6.7]	18.1 [6.0]
AHI (events/h)	3.8 [7.8]	4.2 [8.3]	3.3 [6.4]
AHI < 1 (*n*)	163 (17.2%)	91 (16.0%)	72 (19.1%)
1 ≤ AHI < 5 (*n*)	386 (40.8%)	223 (39.1%)	163 (43.4%)
5 ≤ AHI < 10 (*n*)	172 (18.2%)	111 (19.5%)	61 (16.2%)
AHI ≥ 10 (*n*)	225 (23.8%)	145 (25.4%)	80 (21.3%)

Data presented as median [interquartile range] or n (%).
BMI = body mass index, AHI = apnea-hypopnea index.

Table 1. Clinical and demographic data of the children involved in the study.

AHI cut-off	Model	Se (%) [95%CI]	Sp (%) [95%CI]	Acc (%) [95%CI]	AUC [95%CI]	LR+ [95%CI]	LR- [95%CI]
1 event/h	**MLP^{AF}**	94.07 [a,b] [92.44,95.57]	11.16 [a,b] [6.65,15.70]	78.14 [a,b] [75.67,80.61]	0.72 [a,b] [0.68,0.76]	1.06 [a,b] [1.01,1.13]	0.58 [a,b] [0.40,1.91]
	MLP^{AF,ODI3}	98.03 [a,c] [97.07,98.93]	15.27 [a,c] [9.90,20.48]	82.16 [a,c] [79.83,84.44]	0.82 [a,c] [0.79,0.84]	1.16 [a,c] [1.09,1.25]	0.14 [a,c] [0.07,0.39]
	***ODI*3**	59.78 [b,c] [56.66,63.32]	86.06 [b,c] [80.83,90.79]	64.81 [b,c] [61.89,67.97]	0.82 [b,c] [0.79,0.85]	4.59 [b,c] [3.52,10.83]	0.47 [b,c] [0.42,0.52]
5 events/h	**MLP^{AF}**	78.66 [a,b] [74.56,83.18]	50.61 [a,b] [46.95,54.65]	61.20 [a,b] [58.17,64.21]	0.72 [a,b] [0.68,0.75]	1.60 [a,b] [1.47,1.78]	0.42 [a,b] [0.33,0.52]
	MLP^{AF,ODI3}	81.56 [a,c] [77.58,85.73]	83.00 [a,c] [79.95,85.92]	82.49 [a,c] [80.08,84.77]	0.88 [a] [0.86,0.91]	4.85 [a,c] [4.20,6.37]	0.22 [a,c] [0.17,0.27]
	***ODI*3**	69.45 [b,c] [64.63,74.16]	89.38 [b,c] [86.91,91.68]	81.88 [b,c] [79.54,84.25]	0.88 [b] [0.86,0.90]	6.68 [b,c] [5.60,10.17]	0.34 [b,c] [0.29,0.40]
10 event/h	**MLP^{AF}**	55.85 [a,b] [49.64,62.78]	83.16 [a,b] [80.56,85.64]	77.35 [a,b] [74.74,79.96]	0.76 [a,b] [0.72,0.79]	3.36 [a,b] [2.80,4.30]	0.53 [a,b] [0.45,0.61]
	MLP^{AF,ODI3}	72.29 [a,c] [66.28,78.12]	94.98 [a,c] [93.48,96.42]	90.15 [a,c] [88.39,92.00]	0.93 [a,c] [0.91,0.95]	15.01 [a,c] [11.82,30.73]	0.29 [a,c] [0.23,0.35]
	***ODI*3**	81.05 [b,c] [75.71,86.12]	88.58 [b,c] [86.34,90.76]	87.00 [b,c] [84.93,89.06]	0.92 [b,c] [0.90,0.94]	7.23 [b,c] [6.10,9.98]	0.21 [b,c] [0.16,0.27]

AHI = apnea-hypopnea index, Se = sensitivity, Sp = specificity, Acc = accuracy, AUC = area under receiver-operating characteristic curve, LR+ = positive likelihood ratio, LR- = negative likelihood ratio, 95%CI = 95% confidence interval, *ODI*3 = 3% oxygen desaturation index, MLP^{AF} = Multi-Layer perceptron neural network whose inputs are B_{min}, BE_1, H_2, and fm_2 (minimum amplitude, bispectral entropy of first order, sum of logarithmic amplitudes of diagonal elements of bispectrum, and coordinate *y* of the weighted center of bispectrum, respectively), MLP^{AF,ODI3} = Multi-Layer perceptron neural network whose inputs are BE_1, H_2, and fm_2, and *ODI*3, [a] Significant differences (*p*-value < 0.001) between MLP^{AF} and MLP^{AF,ODI3} using Mann-Whitney *U* test with Bonferroni correction, [b] Significant differences (*p*-value < 0.001) between MLP^{AF} and *ODI*3 using Mann-Whitney *U* test with Bonferroni correction, [c] Significant differences (*p*-value < 0.001) between MLP^{AF,ODI3} and *ODI*3 using Mann-Whitney *U* test with Bonferroni correction.

Table 2. Diagnostic performance of MLP^{AF} and MLP^{AF,ODI3} models, and *ODI*3 in the test set for the AHI cut-offs 1, 5, and 10 events/h.

Model	*k* [95%CI]	ICC [95%CI]	Acc_4(%) [95%CI]
MLP^{AF}	0.14 [0.11,0.18] [a,b]	0.52 [0.41,0.59] [a,b]	37.08 [34.17,40.15] [a,b]
$MLP^{AF,ODI3}$	0.38 [0.34,0.42] [a,c]	0.88 [0.81,0.91] [a]	57.94 [55.02,61.09] [a,c]
***ODI*3**	0.29 [0.26,0.33] [b,c]	0.88 [0.82,0.90] [b]	46.21 [43.39,49.60] [b,c]

k = Cohen's kappa, ICC = intra-class correlation coefficient, Acc_4 = four-class accuracy, 95%CI = 95% confidence interval, *ODI*3 = 3% oxygen desaturation index, MLP^{AF} = Multi-Layer perceptron neural network whose inputs are B_{min}, BE_1, H_2, and fm_2 (minimum amplitude, bispectral entropy of first order, sum of logarithmic amplitudes of diagonal elements of bispectrum, and coordinate *y* of the weighted center of bispectrum, respectively), $MLP^{AF,ODI3}$ = Multi-Layer perceptron neural network whose inputs are BE_1, H_2, and fm_2, and *ODI*3. [a] Significant differences (*p*-value < 0.001) between MLP^{AF} and $MLP^{AF,ODI3}$ using Mann-Whitney *U* test with Bonferroni correction, [b] Significant differences (*p*-value < 0.001) between MLP^{AF} and *ODI*3 using Mann-Whitney *U* test with Bonferroni correction, [c] Significant differences (*p*-value < 0.001) between $MLP^{AF,ODI3}$ and *ODI*3 using Mann-Whitney *U* test with Bonferroni correction.

Table 3. Global performance of MLP^{AF} and $MLP^{AF,ODI3}$ models, and *ODI*3 in the test set.

Study	Nº Subjects (Total dataset/Test set)	Signal	Methods (Analysis/Selection/Classification)	AHI cut-off (events/h)	Se (%)	Sp (%)	Acc (%)	AUC
Shouldice *et al*. (2004) [8]	50/25	ECG	Temporal and spectral analysis / - / QDA	1	85.70	81.80	84.00	0.83
Gil *et al*. (2010) [9]	21/21	PPG	Analysis of HRV, PTTV, and DAP events / Wrap method / LDA	5	75.00	85.70	80.00	-
Tsai *et al*. (2013) [52]	148/148	SpO_2	*ODI*4 / - / -	1	77.70	88.90	79.00*	0.86
				5	83.80	86.50	85.10*	0.91
				10	89.10	86.00	87.10*	0.94
Dehkordi *et al*. (2016) [51]	146/146	PPG	Temporal, spectral, and detrended fluctuation analysis / LASSO / LASSO	5	76.00	68.00	71.00	0.78
Hornero *et al*. (2017) [31]	4191/3602	SpO_2	Statistical, spectral, non-linear analysis, and *ODI*3 / FCBF / MLP	1	84.02	53.19	75.15	0.79
				5	68.16	87.19	81.65	0.85
				10	68.66	94.07	90.17	0.91
Barroso-García *et al*. (2017) [14]	501/251	AF	Spectral entropies and central tendency measure / FSLR / LR	1	60.50	58.60	60.00	0.59
				5	65.00	80.60	76.00	0.78
				10	83.30	79.00	80.00	0.80
Vaquerizo-Villar *et al*. (2018) [12]	298/75	SpO_2	Anthropometric variables, *ODI*3, spectral and bispectral analysis / FCBF / MLP	5	61.76	97.56	81.33	-
				10	60.00	94.54	85.33	-
Xu *et al*. (2019) [43]	432/432	SpO_2	*ODI*3 and 3rd statistical moment of the spectral band of interest / FCBF / MLP	1	95.34	19.10	79.63	0.78
				5	77.78	80.46	79.40	0.87
				10	73.53	92.73	88.19	0.90
Garde *et al*. (2019) [53]	207/207	SpO_2 PRV	Temporal and spectral analysis / Stepwise-selection / LR	1	80.00	65.00	75.00	0.80
				5	85.00	79.00	82.00	0.89
				10	82.00	91.00	89.00	0.92
Barroso-García *et al*. (2020) [13]	946/376	AF *ODI*3	Recurrence quantification analysis and *ODI*3 / FCBF / BY-MLP	1	97.70	22.22	83.24	0.81
				5	78.72	78.30	78.46	0.88
				10	78.75	94.26	90.96	0.93
Jiménez-García *et al*. (2020) [15]	974/390	AF SpO_2	Statistical, non-linear, spectral analysis, and *ODI*3 / FCBF / Multiclass AdaBoost	1	92.06	36.00	81.28	-
				5	76.03	85.66	82.05	-
				10	62.65	97.72	90.26	-
This study	**946/376**	**AF *ODI*3**	**Bispectral analysis and *ODI*3 / FCBF / MLP**	**1**	**98.03**	**15.27**	**82.16**	**0.82**
				5	**81.56**	**83.00**	**82.49**	**0.88**
				10	**72.29**	**94.98**	**90.15**	**0.93**

QDA = Quadratic discriminant analysis, HRV = Heart rate variability, PTTV = Pulse transit time variability, DAP = Decreases in amplitude fluctuations of the PPG signal, LDA = Linear discriminant analysis, *ODI*4 = 4% oxygen desaturation index, LASSO = Least absolute shrinkage and selection operator, *ODI*3 = 3% oxygen desaturation index, FCBF = Fast correlation based filter, MLP = Multi-Layer perceptron neural network, FSLR = Forward stepwise logistic regression, LR = Logistic regression model, PRV = Pulse rate variability, BY-MLP = Multi-Layer perceptron neural network with Bayesian approach. *Computed from reported data.

Table 4. Diagnostic performance of state-of-the-art approaches in the childhood OSA context.

FIGURES:

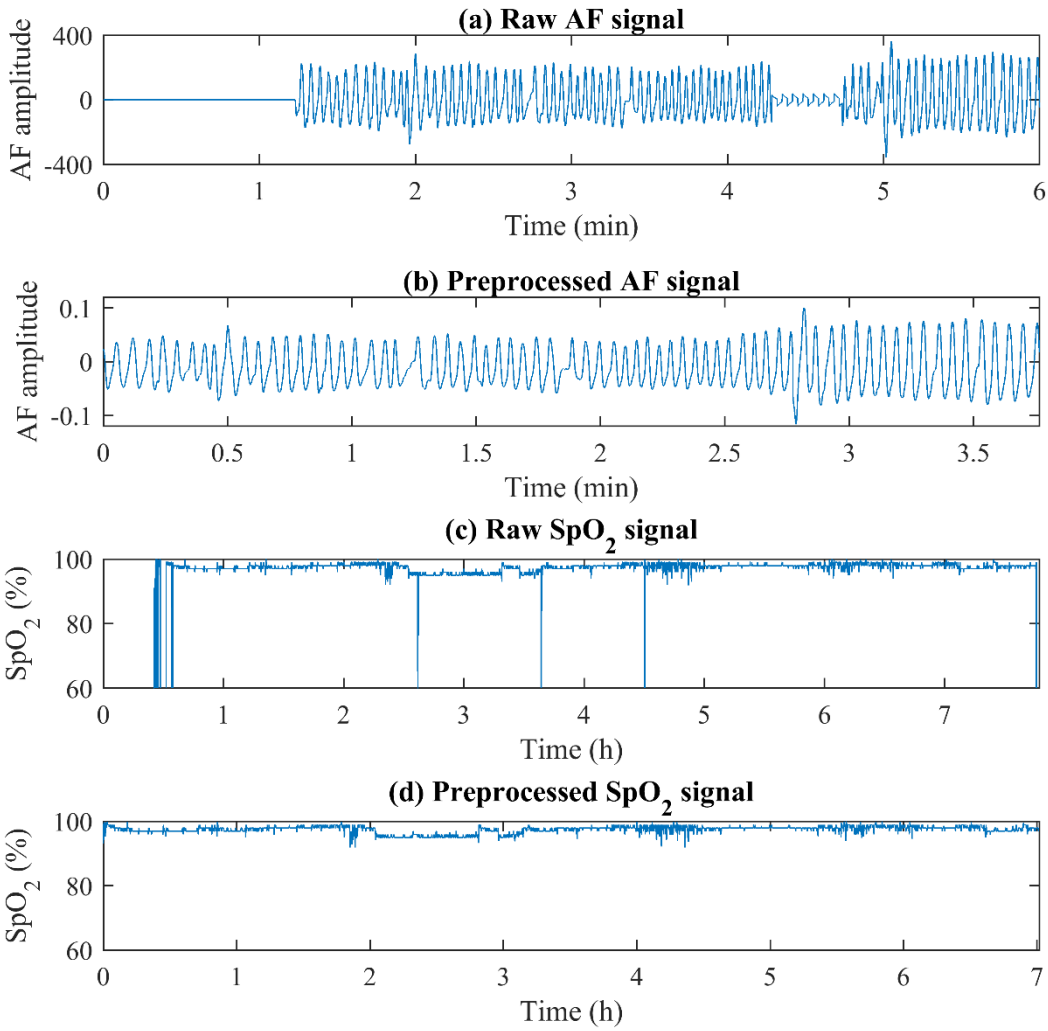

Figure 1. Airflow signal (AF): (a) before and (b) after the preprocessing stage, and blood oxygen saturation signal (SpO_2): (c) before and (d) after the preprocessing stage.

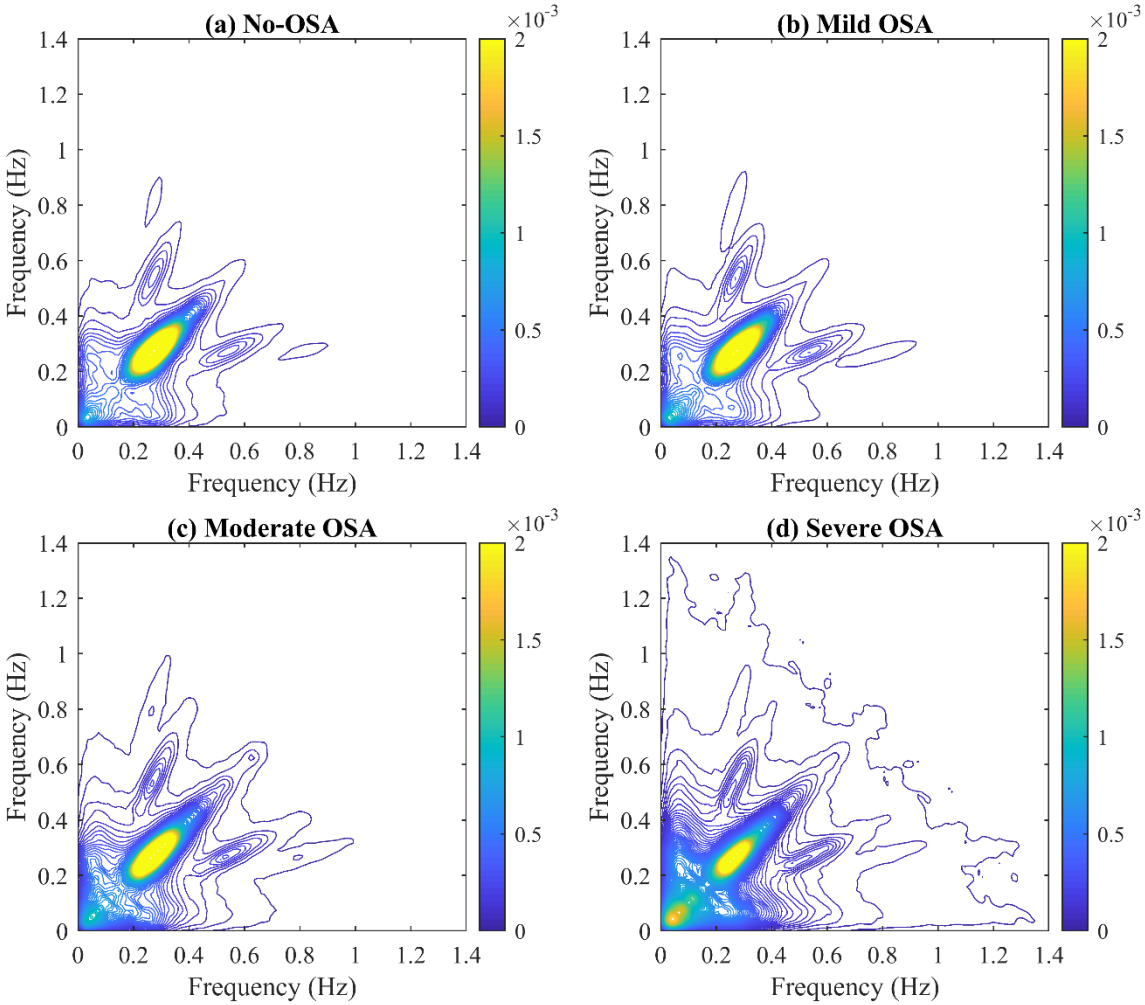

Figure 2. Contour of the averaged normalized bispectrum of the groups (a) no-OSA, (b) mild OSA, (c) moderate OSA, and (d) severe OSA in the training set.

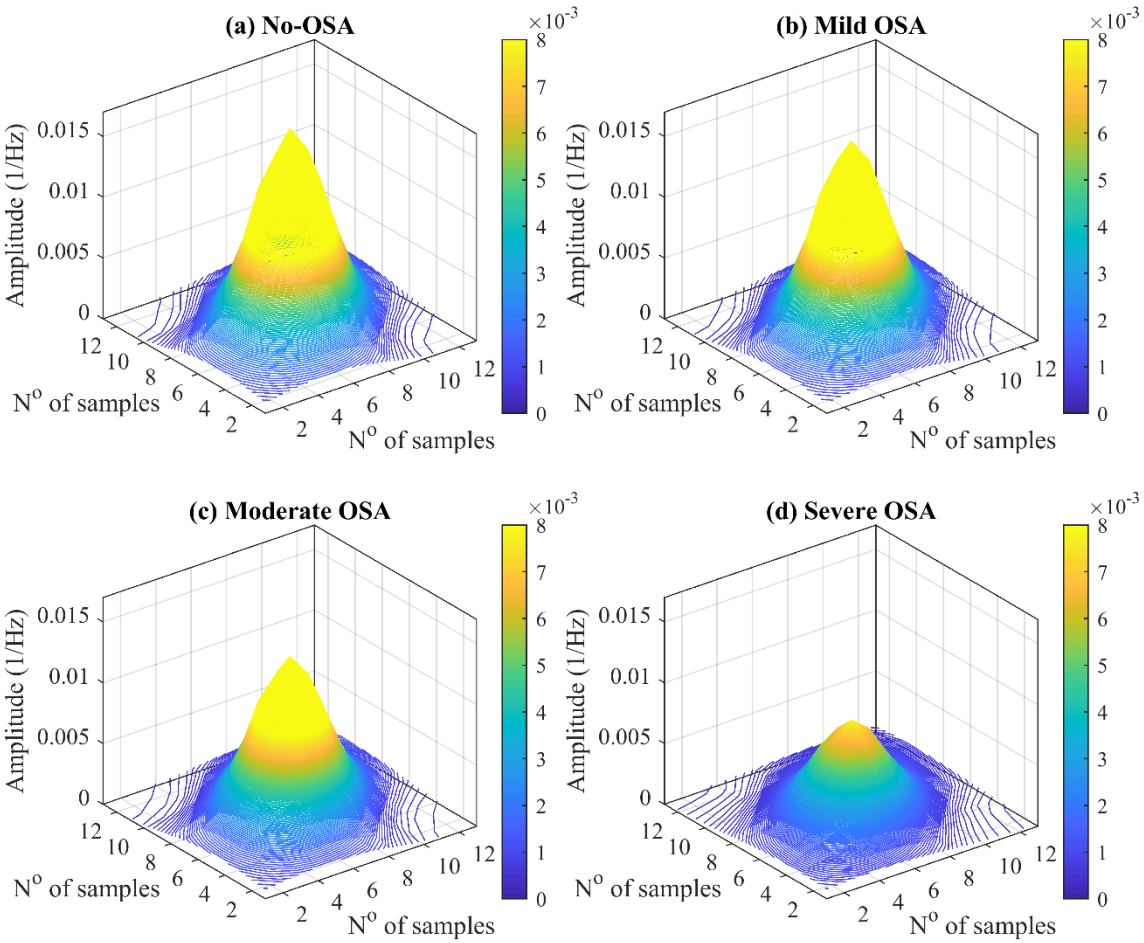

Figure 3. Contour 3D of the averaged bispectral adaptive band of the groups (a) no-OSA, (b) mild OSA, (c) moderate OSA, and (d) severe OSA in the training set.

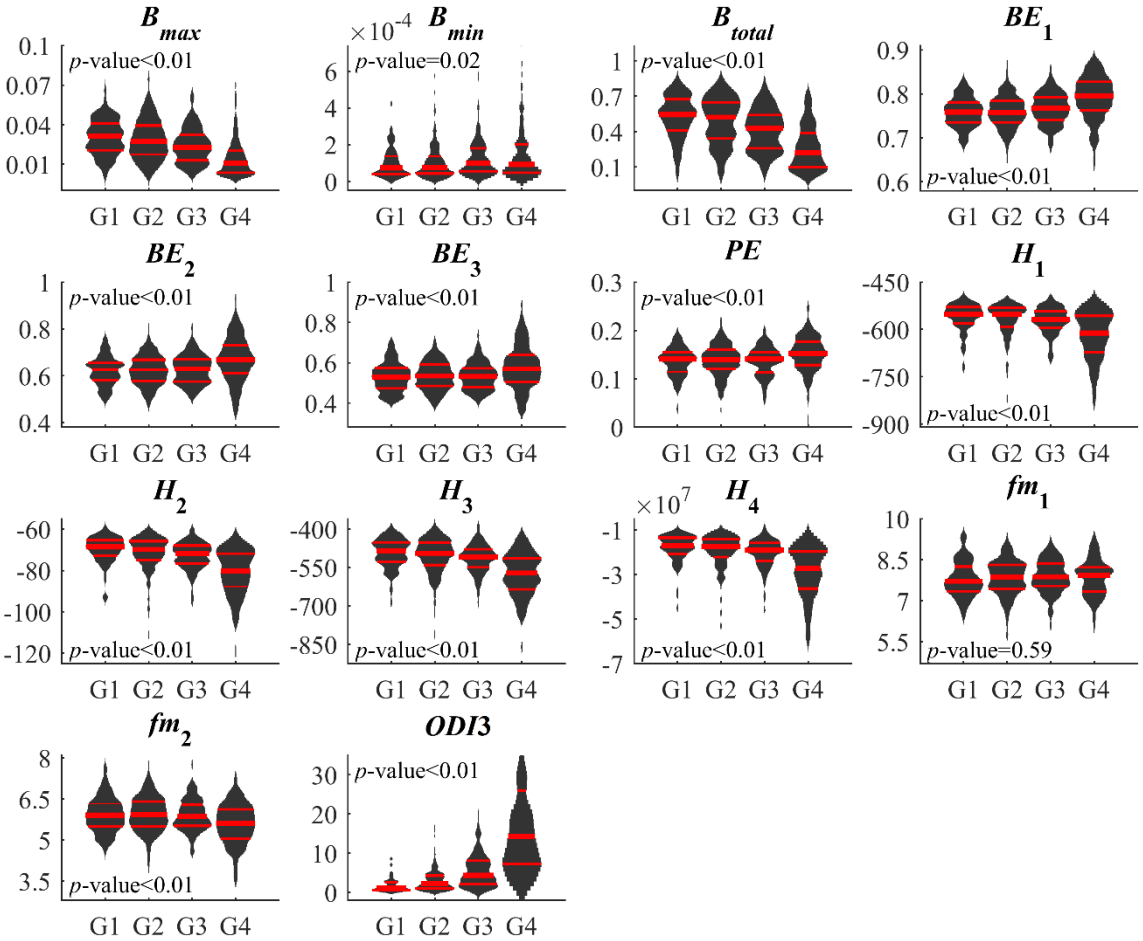

Figure 4. Violin plots of the 13 bispectral features and *ODI*3 extracted from the groups no-OSA (G1), mild OSA (G2), moderate OSA (G3), and severe OSA (G4) in the training set.

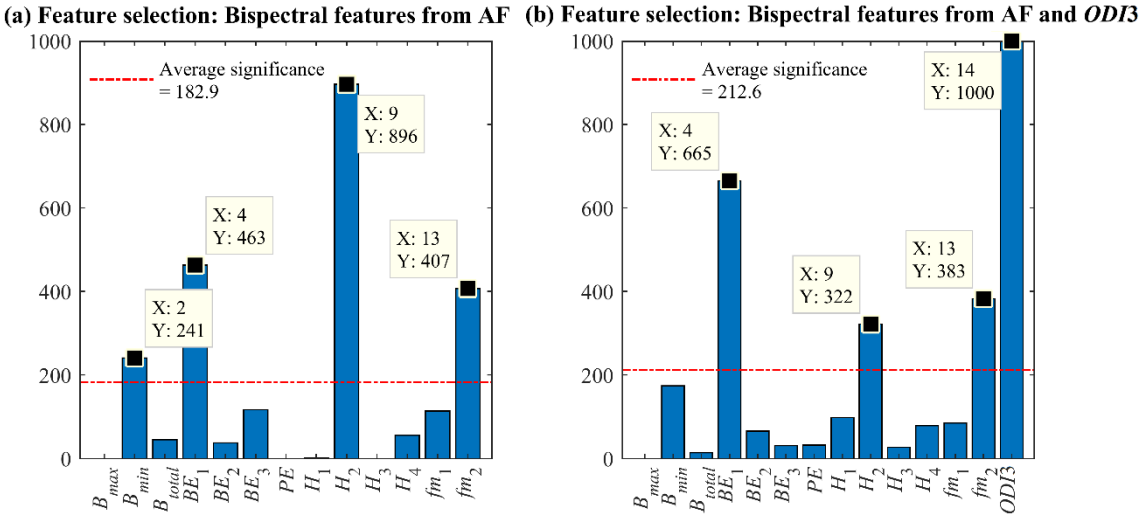

Figure 5. Results of feature selection with the training set using Fast Correlation-Based Filter in 1000 bootstrap: (a) bispectral features from AF and (b) bispectral features from AF and *ODI*3.

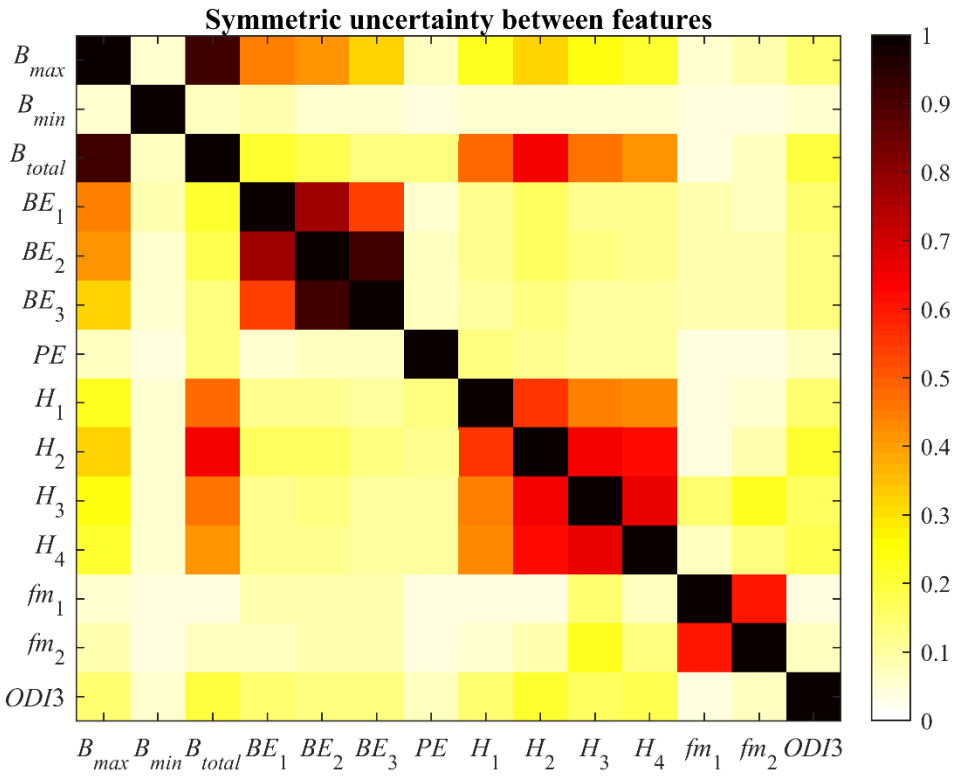

Figure 6. Heat map of the symmetric uncertainty between the extracted features. A version with the 95% confidence intervals is included in the supplementary material.